Microstructure evolution during solid-state foaming of titanium

N.G.D. Murray[1], D.C. Dunand*

Northwestern University, Department of Materials Science and Engineering, 2220 Campus Dr., Evanston, IL 60208, USA

Abstract

Solid-state foaming of commercially pure titanium was achieved by high-temperature expansion of high-pressure argon bubbles trapped in titanium by a powder-metallurgy technique. The foaming step was performed at constant temperature, where creep of the titanium matrix controls pore expansion, or during thermal cycling around the α/β allotropic temperature, which induces transformation superplasticity of the matrix. Superplastic foaming led to significantly faster pore growth and higher terminal porosity than isothermal creep foaming. During thermal cycling, the porosity remains nearly fully closed to the surface of the specimen up to the point where the maximum porosity (44%) is obtained, despite the presence of some internal pore coalescence. With continued thermal cycling, pores coalesce further by fracture of thin interpore walls and pores finally open to the surface, but without a significant increase in the amount of total porosity. The remnants of these walls result in a jagged pore morphology. Under isothermal conditions, pores remain small, equiaxed and unconnected with no pore surface roughness. However, after long annealing times, they exhibit faceting due to surface diffusion.
© 2003 Elsevier Ltd. All rights reserved.

Keywords: A: Metals; A: Foams; B: Creep; B: Porosity; E: Powder processing

1. Introduction

Because titanium and its alloys exhibit excellent mechanical properties, low density and high chemical resistance, titanium-based foams have potential engineering applications for load-bearing sandwich cores in the aerospace, naval and ground transportation industries [1,2] and as porous implants in the biomedical industry, for which the excellent biocompatibility and fatigue properties of titanium-based materials are also essential [1–5]. The high melting temperature and strong chemical reactivity of titanium make solid-state foaming more promising [6–8] than liquid state foaming techniques used, e.g., for aluminum [1,2].

Solid-state foaming was first described by Kearns et al. [6–8] and later by others [9,10–13] for the titanium alloy Ti-6Al-4V, and by us for unalloyed titanium [14]. The foaming process, as described in Refs [8–14], and schematically depicted in Fig. 1, starts with Hot Isostatic Pressing (HIPing) titanium powder in the presence of argon gas. The resulting compacted material consists of a continuous titanium matrix containing a small volume fraction of discreet, micron-sized, high-pressure argon pores. On exposure to elevated temperatures, these bubbles expand by creep of the surrounding metal due to the high argon pressure. Kearns et al. [6–8] achieved porosities of up to ∼40% in Ti-6Al-4V after heat treatments at very high temperatures (1240 °C) and long hold times (several days). The growth rate of the pores was controlled by the slow creep deformation of the metal and the amount of argon gas entrapped during HIPing.

In a previous publication [14], we demonstrated that deformation of the titanium matrix surrounding the high-pressure argon pores could be enhanced using transformation superplasticity (TSP), thus significantly increasing overall foaming rates and total porosity. Transformation superplasticity is exhibited by polymorphic materials and their alloys (e.g. titanium [15–17], Ti-6Al-4V [18–20] and many other polymorphic metals and alloys [15,21]), and is driven by the density difference between the two allotropic phases. As these two phases coexist during the phase transformation, internal mismatch strains develop. The mismatch strains are biased by an externally-applied stress, which results in a net strain increment in the direction of the biasing stress during each phase transformation. By repeatedly cycling through the phase transformation, tensile elongations well in excess of 100% can be accumulated without

---

[1] Formally N.G. Davis
* Corresponding author. Tel.: +1-847-491-5370; fax: +1-847-467-6573.
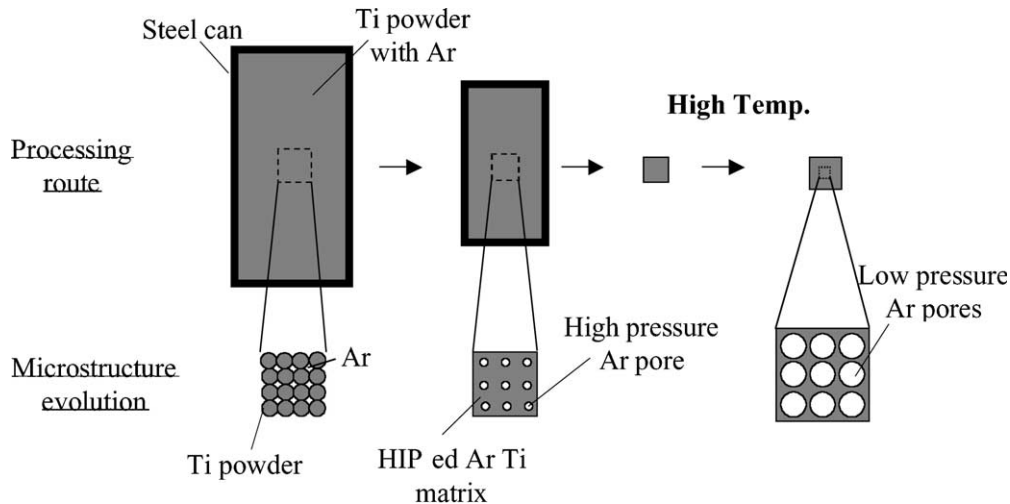 *E-mail address:* dunand@northwestern.edu (D.C. Dunand).

Fig. 1. Schematic of foaming process, where titanium powders are compacted by HIPing in the presence of argon and the resulting high-pressure argon bubbles then expand under low-pressure argon atmosphere at high temperature.

fracture or cavitation during uniaxial stress tests of fully dense materials.

Using the argon pressure within the pores of foams as the biasing stress, we demonstrated that foaming titanium under superplasticity-dominated conditions by thermal cycling about the allotropic temperature leads to faster foaming rates and higher terminal porosities than under isothermal conditions, where the deformation is dominated by creep [14]. In the present paper, we investigate the evolution of pore fraction, connectivity and morphology during solid-state foaming under both isothermal (creep) conditions and thermal-cycling (superplastic) conditions.

2. Experimental procedures

Spherical titanium powders of commercial purity (CP-Ti, from Starmet, Concord, MA) were sieved to $-200/+230$ mesh (62–88 μm average of 75 μm), packed in a mild-steel can, backfilled with 3.3 atm argon and HIPed at 890 °C for 120 min under a pressure of 100 MPa, using a HIP by Connaway Technologies and Isostatic Forging (Hilliard, OH). Cubic specimens were produced by electro-discharge machining with 9 mm edges. These specimens were foamed in a flowing Ar atmosphere at 1 atm pressure. For superplastic foaming experiments, specimens were thermally cycled with a 4-min cycle period between 830 and 980 °C, spanning the allotropic temperature range of CP-Ti (nominally 882 °C, but expected to be higher and wider due to oxygen content [22]). Isothermal foaming experiments were performed at 903 °C, the effective temperature of the above thermal cycle.

The effective temperature is defined as the temperature at which the isothermal creep rate is the same as the time-averaged creep rate during thermal cycling in the absence of TSP [17,18]. The effective temperature was determined by finding the time-average creep rate of the thermal cycle used to induce TSP in the experiments described above, using the lattice activation energies for power-law creep given in Ref. [23] for α-Ti and β-Ti. Due to the low creep rate of α-Ti, the effective temperature is fortuitously close to the arithmetic mean of the thermal cycle. Thus, by comparing foaming kinetics during thermal cycling between 830 and 980 °C and during isothermal foaming at 903 °C, the effect of TSP is directly revealed.

Frequent excursions to room temperature occurred to determine specimen porosity by Archimedes density measurements in distilled water. A thin layer of vacuum grease was used to seal the specimen surface to prevent infiltration of water into any open porosity, yielding a direct measurement of the total porosity. Density measurements were also performed using helium pycnometry on unsealed specimens, allowing for direct measurement of closed porosity. Open porosity was calculated as the difference of these two measurements.

For metallographic examination, specimens were cut in half along one of the cube face diagonals using a low-speed diamond saw, mounted in acrylic resin and polished to 0.05 μm alumina. Foamed specimens were vacuum-infiltrated with the same acrylic resin used for mounting at intervals during polishing, in order to fill open porosity and retain the original pore shape during polishing.

3. Results

Fig. 2(a) shows total, open and closed specimen porosity as a function of time during the first 83 h of foaming under thermal cycling conditions for a single specimen. During the early stages of thermal cycling,
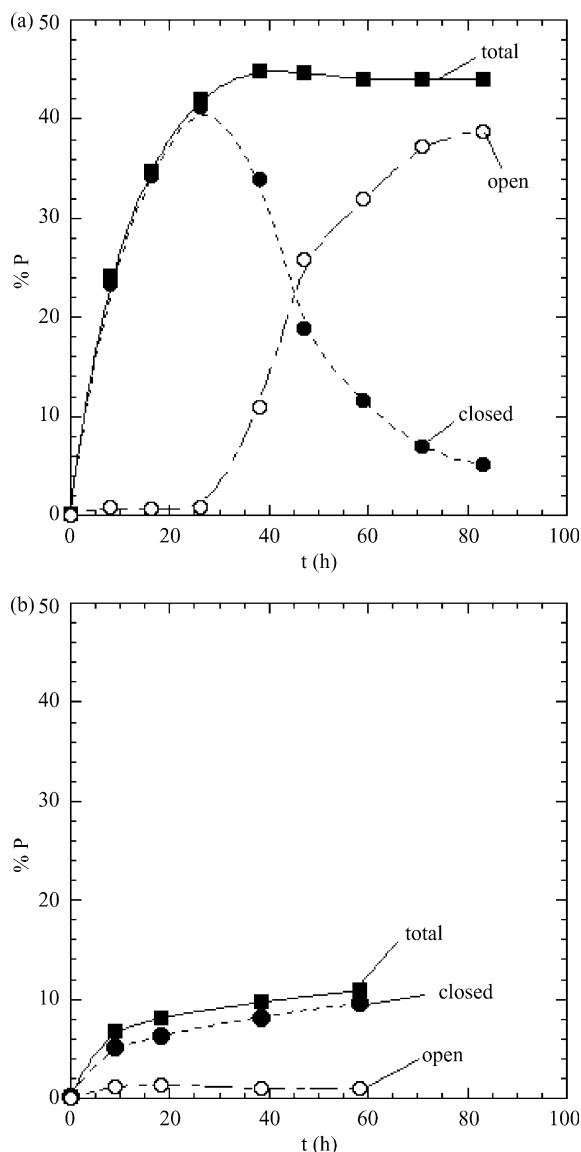
Fig. 2. Total, open and closed porosity as a function of time during (a) thermal cycling (830–980 °C) and (b) isothermal foaming (903 °C).

the total porosity increases rapidly with time. Up to a total porosity $p = 42\%$ (achieved after 26 h of thermal cycling), the porosity remains almost entirely closed. Upon further thermal cycling, pores open rapidly while the total porosity only increases from $p = 42\%$ to $p = 44\%$. Upon reaching a final open porosity ratio (defined as the ratio of open porosity to total porosity) $F = 0.88$ after 83 h of foaming, the rate of pores opening to the specimen surface has tapered off significantly. Due to concerns with specimen oxygen contamination which compromises the transformation temperature, thermal cycling was not continued to saturation of open porosity. Fig. 2(b) shows total, open and closed porosity as a function of time for isothermal foaming at 903 °C, resulting in much slower foaming kinetics ($p = 11\%$ after 58 h) and nearly fully closed pores ($F = 0.05$).

Optical micrographs from additional specimens foamed under the same conditions as in Fig. 2(a) are shown in Fig. 3(a–d) to illustrate the pore morphology evolution during four steps of foaming by thermal cycling. Total porosity, p, and open porosity ratio, F, were measured independently for each of these four specimens. Fig. 3(a) shows the pore structure for the as-HIPed material and Fig. 3(b–d) show the pore structure after 8 h ($p = 23\%$, $F = 0.04$), 26 h ($p = 39\%$, $F = 0.10$), and 83 h ($p = 44\%$, $F = 0.88$), respectively. The very small pores in the as-HIPed state (about 6 μm in diameter, Fig. 3(a)) grow rapidly in the first 8 h of cycling, resulting in much larger pores close to 100 μm in diameter, which are mostly rounded and generally equiaxed, Fig. 3(b). During the following 18 h of thermal cycling, Fig. 3(b) and (c), both pore size and total porosity vary much less rapidly than in the first 8 h. However, noticeable pore coalescence is observed after 26 h, Fig. 3(c), despite the small amount of measured open porosity ($F = 0.05$), suggesting that internal pore coalescence occurs well before an appreciable amount of porosity opens to the surface. Additionally, coalesced pores after 26 h are much less rounded than after 8 h. As expected, the pores are not aligned in any particular direction and remain randomly distributed. The pore morphology changes considerably between 26 h of thermal cycling, Fig. 3(c), and 83 h of thermal cycling, Fig. 3(d), despite only a modest change in total porosity from $p = 39\%$ to $p = 44\%$. The mostly equiaxed, rounded shape of the pores becomes very jagged and rough. Furthermore, the amount of open porosity has greatly increased, with an open porosity ratio increasing from $F = 0.10$ to $F = 0.88$. Finally, pore dimensions of up to 500 μm are observed in Fig. 3(d) as compared to ca.150 μm in Fig. 3(c).

Fig. 4(a–c) show examples of very thin inter-pore regions and long, interconnected pores in the specimen cycled for 83 h (shown in Fig. 3(d)). Thin pore walls (~15 μm), which result from large deformation of the originally thick inter-pore regions (on the order of the powder size, ~75 μm), are shown in Fig. 4(a). Fig. 4(b) shows freshly ruptured walls protruding into the larger pore formed by coalescence of two adjacent pores. Fig. 4(c) shows a series of interconnected, coalesced pores, which have created highly elongated (but not aligned) channels. As the relative open porosity ratio increases, these elongated channels became more prevalent. While two-dimensional metallurgical cross-sections do not allow for an assessment of the real three-dimensional pore structure and connectivity, it is very likely that the channels visible in Fig. 4(a–c) are connected to other channels outside the plane of polish, given the high fraction of open porosity.

Finally, Fig. 5 is an optical micrograph of the foam isothermally processed for 58 h at 903 °C, whose porosity is reported in Fig. 2(b).The original pores present

before foaming (shown in Fig. 3(a)) have increased in size, but remained discreet and equiaxed, with very little coalescence after 58 h of isothermal foaming. Significant pore faceting is present, as noted by the arrow in Fig. 5.

4. Discussion

Solid-state foaming by isothermal creep expansion of high-pressure argon bubbles results in slow foaming rates and low porosities, even at a relatively high homologous temperature $T/T_m = 0.61$ where the creep strength of titanium is low [24]. Neglecting the small variation in pore pressure due to thermal cycling, the substantial enhancement in foaming rate due to TSP can be directly assessed by comparing with the rate during isothermal foaming at the effective temperature (Fig. 2(a) and (b)). Such an enhancement due to TSP is in qualitative agreement with results from a previous TSP foaming study [14], and was also observed for the uniaxial [17,19,20] and multi-axial [18–20,25] deformation of non-porous specimens of CP-Ti and Ti-6Al-4V.

Modeling of the foaming rates will be presented in future publications.

At low porosity levels ($p < 25\%$), both methods of pore expansion yield foam that exhibits equiaxed pores without interconnectivity, as shown in Fig. 3(b) ($p = 23\%$ after 8 h TSP foaming) and Fig. 5 ($p = 11\%$ after 58 h isothermal foaming). The main difference is the pore faceting exhibited by the isothermally-foamed specimen. Faceting was also observed during the first studies of isothermal foaming of β-phase Ti-6Al-4V by Kearns et al. [6–8] who reported pores with a similar size to those in Fig. 5(b) but higher volume fractions (up to ca. 40%), after isothermal foaming for the same length of time (60 h) but at much higher temperatures (1240 °C). These authors attributed the faceting to low-energy {100} surfaces growing by surface diffusion at the expense of higher-energy surfaces. This faceting, which is also observed during thermal etching, controls the shape of the pores only when pore expansion, which favors a spherical shape at low porosity levels (as in the present case), is very slow. However, a direct comparison with Ti-6Al-4V is not possible because of the
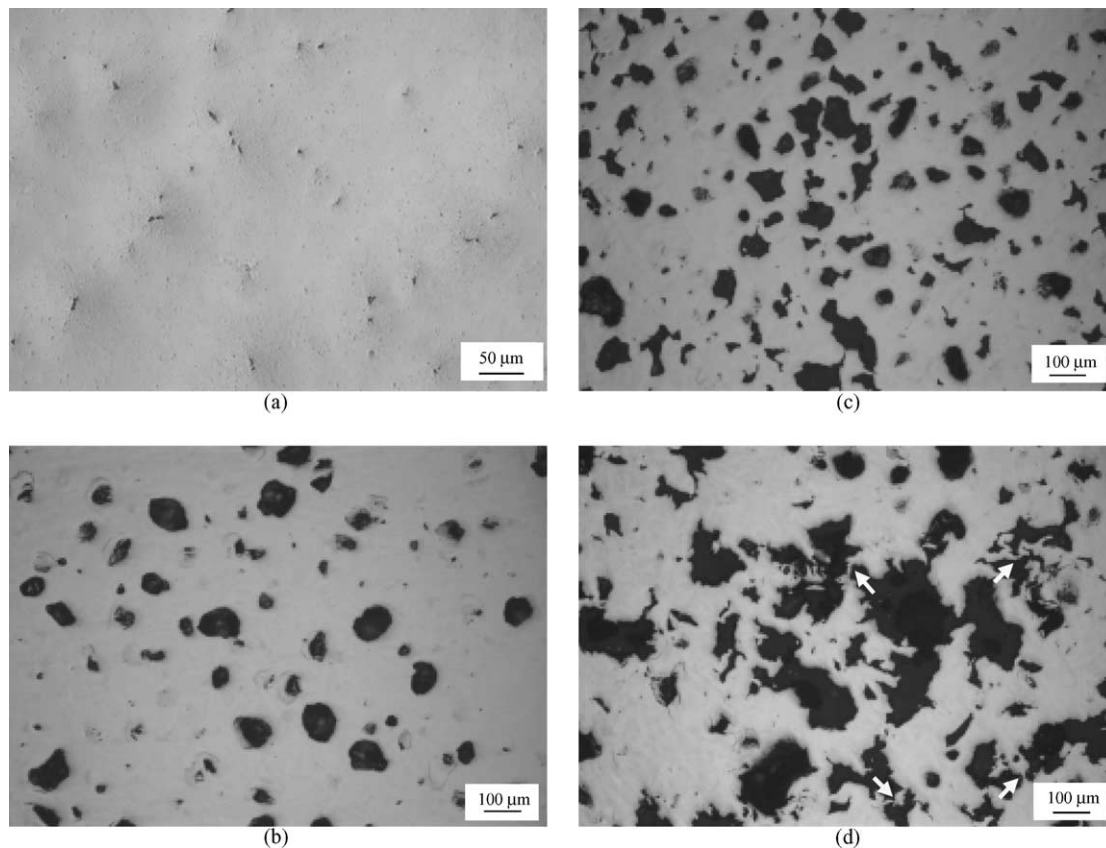

Fig. 3. Optical micrograph showing pore morphology evolution with pore growth and opening of porosity as a function of time during superplastic thermal cycling (830–980 °C); (a) 0 h, as-HIPed state (total porosity, $p = 0.14\%$, relative open porosity ratio, $F = 0$), (b) 8 h ($p = 23\%$, $F = 0.04$), (c) 26 h ($p = 39\%$, $F = 0.10$) and (d) 83 h ($p = 44\%$, $F = 0.88$). Arrows in (d) show very thin interpore regions achievable under superplastic

higher creep strength of Ti-6Al-4V and its different transformation temperatures and kinetics as compared to CP-Ti.

At higher porosity levels ($p > 25\%$) attained only during TSP foaming, pore coalescence occurs through rupture of very thin walls between the pores. Further increase in total porosity is due to continued growth of individual pores, or clusters of connected pores, containing pressurized argon. Pore coalescence by itself does not increase the total porosity (unless secondary mechanisms become activated, e.g. stress concentrations) but the fracture of the pore walls leads to a marked changed in the pore morphology. Such thin walls were made possible by the high ductility achievable during TSP, as shown by arrows in Figs. 3(d) and 4(b). Fractured thin walls become protrusions within the coalesced pores, giving them a jagged morphology. The only mechanism by which these protrusions can shrink is diffusion, which is too slow to markedly spheroidize the pores for the temperatures and times used in the present study. This explains the noticeable

difference in pore morphology, shape and size between Fig. 3(c) and (d), for which there is only a small change in total porosity.

The observed decrease in foaming rate is likely due to both the decrease in the pressure of growing pores unconnected to the specimen surface, and the increasing fraction of surface-connected pores (measured as open porosity) whose pressurized argon escaped to the ambient atmosphere and which have thus no driving force for further expansion. With continued thermal cycling, the total porosity remained unchanged but the amount of open porosity increased. This continued opening of porosity to the specimen surface is likely due to the fracture of the very thin pores walls during the thermal cycle, which break without substantially increasing the size of pores because TSP allows for significant deformation even at very low stresses. An increase in the fraction of open porosity is beneficial for biomedical bone-replacement implants for which an interconnected porous structure is desired for bone in-growth, resulting in superior implant fixation.
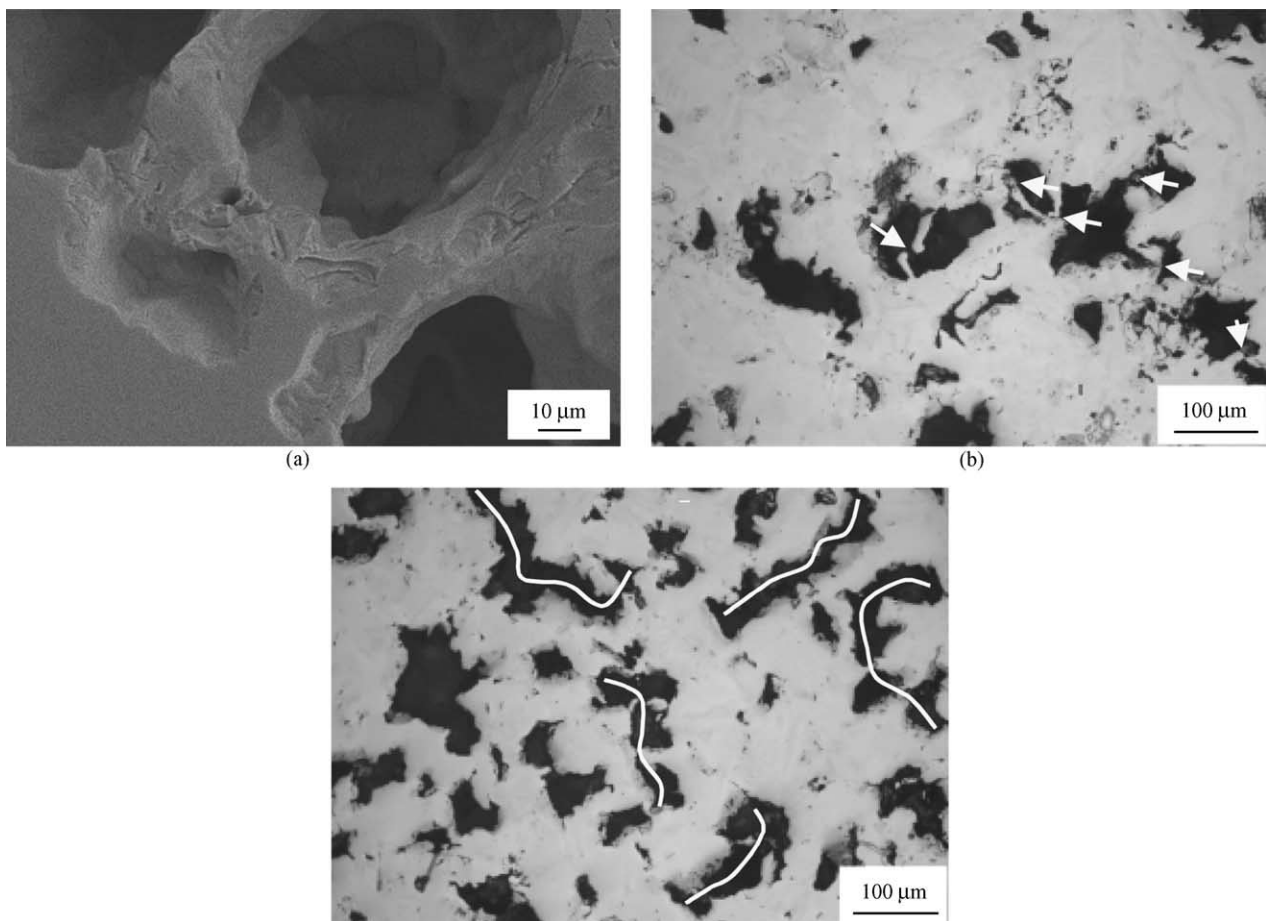

Fig. 4. Micrographs for foam after thermal cycling for 83 h ($p = 44\%$, $F = 0.88$), showing (a) very thin inter-pore regions that are still intact, (b) inter-pore regions that have just ruptured, causing pore coalescence, and very jagged pore shapes, and (c) long channels consisting of interconnected, coalesced pores.
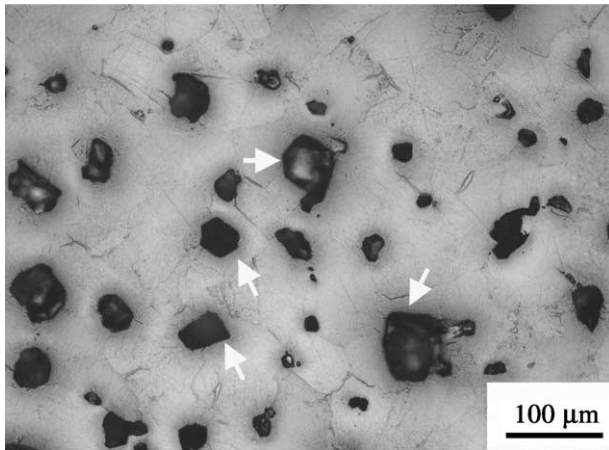
Fig. 5. Microstructure resulting from isothermal foaming at 903 °C for 58 h resulting in 11% total porosity and a relative open porosity ratio, $F = 0.05$. Examples of facetted pores are marked by arrows.

5. Conclusions

The microstructure resulting from solid-state expansion of small, argon-filled pores in CP-Ti (produced by consolidation of 75 μm titanium powders with argon gas) was studied for foaming performed under isothermal or thermal cycling conditions. The following conclusions can be drawn:

1. Under isothermal foaming conditions (903 °C) where creep of the titanium matrix controls foaming rates, pores remain relatively small and spheroid in shape, but become faceted after long times (58 h) due to anisotropic surface energy.

2. Foaming under thermal cycling conditions (830–980 °C), for which transformation superplasticity is the active deformation mechanism, causes pores to grow much faster than under isothermal, creeping conditions, and also result in higher final porosity.

3. Under thermal cycling conditions, most of the porosity remains closed to the surface when the maximum total porosity (44%) is achieved because of the high ductility achievable during superplastic deformation, preventing extensive pore wall fracture. However, limited internal pore coalescence takes place.

4. With further thermal cycling, opening of porosity to the specimen surface occurs, but without significant increase in total porosity; pores coalesce by rupture of interpore walls, with their remnants creating a jagged pore morphology. With continued thermal cycling, large-scale pore coalescence

is observed, resulting in channels with a length of at least 300 μm.

References

[1] Banhart J. Progr Mater Sci 2001;46:559.
[2] Ashby MF, Evans A, Fleck NA, Gibson LJ, Hutchinson JW, Wadley HNG. Metal foams—a design guide. Woburn, MA: Butterworth-Heinemann; 2000.
[3] Donachie MJ. Adv Mater Proc 1998;7:63.
[4] Donachie MJ. Introduction to titanium and titanium alloys, in titanium and titanium alloys source book. In: Donachie Jr MJ. OH: ASM, Metals Park; 1982. p. 3.
[5] Simske SJ, Ayers RA, Bateman TA. Mat Sci Forum 1997;250:151.
[6] Kearns MW, Blenkinsop PA, Barber AC, Farthing TW. Metals and Materials 1987;3(2):85.
[7] Kearns MW. Formation of porous bodies. US patent No 4, 659,545;1987.
[8] Kearns MW, Blenkinsop PA, Barber AC, Farthing TW. Int J Powder Metall 1988;24(1):59.
[9] Martin RL. Integral porous-core metal bodies and in situ method of manufacture thereof. US Patent No 5, 564,064;1996.
[10] Queheillalt DT, Choi BW, Schwartz DS, Wadley HNG. Metall Mater Trans 2000;31A(1):261.
[11] Elzey DM, Wadley HNG. Acta Mater 2001;49(5):849.
[12] Queheillalt DT, Gable KA, Wadley HNG. Scripta Mater 2001; 44(3):409.
[13] Vancheeswaran R, Queheillalt DT, Elzey DM, Wadley HNG. Metall Mater Trans 2001;32:1813.
[14] Davis NG, Teisen J, Schuh C, Dunand DC. J Mater Res 2001; 16(5):1508.
[15] Greenwood GW, Johnson RH. Proc Roy Soc 1965;283A:403 London.
[16] Chaix C, Lasalmonie A. Res Mech 1981;2:241.
[17] Dunand DC, Bedell CM. Acta Mater 1996;44(3):1063.
[18] Dunand DC, Myojin S. Mat Sci Engng 1997;230A:25.
[19] Schuh C, Dunand DC. Acta Mater 2001;49(2):199.
[20] Schuh C, Dunand DC. J Mater Res 2001;16(3):865.
[21] Nieh TG, Wadsworth J, Sherby OD. Superplasticity in metals and ceramics. Cambridge, UK: Cambridge University Press; 1997.
[22] Elmer JW, Wong J, Ressler T. Metall Mater Trans 1998;29A:2761.
[23] Frost HJ, Ashby MF. Deformation-mechanism maps: the plasticity and creep of metals and ceramics. Oxford, UK: Pergamon Press; 1982.
[24] Schuh C, Dunand DC. Scripta Mater 2001;45:1415.
[25] Frary M, Schuh C, Dunand DC. Metall Mat Trans 2002; 33A:1669–80.